2D Materials

RECEIVED
11 July 2016

REVISED
15 September 2016

ACCEPTED FOR PUBLICATION
25 November 2016

PUBLISHED
12 December 2016

PAPER

Ultrafast charge transfer between $MoTe_2$ and MoS_2 monolayers

Shudi Pan[1,2], **Frank Ceballos**[2], **Matthew Z Bellus**[2], **Peymon Zereshki**[2] **and Hui Zhao**[2]

[1] College of Physics, Qingdao University, Qingdao, Shandong 266071, People's Republic of China
[2] Department of Physics and Astronomy, The University of Kansas, Lawrence, KS 66045, USA

E-mail: huizhao@ku.edu

Keywords: van der Waals interface, transition metal dicholcogenide, molybdenum ditelluride, charge transfer, transient absorption

Abstract

High quality and stable electrical contact between metal and two-dimensional materials, such as transition metal dichalcogenides, is a necessary requirement that has yet to be achieved in order to successfully exploit the advantages that these materials offer to electronics and optoelectronics. $MoTe_2$, owing to its phase changing property, can potentially offer a solution. A recent study demonstrated that metallic phase of $MoTe_2$ connects its semiconducting phase with very low resistance. To utilize this property to connect other two-dimensional materials, it is important to achieve efficient charge transfer between $MoTe_2$ and other semiconducting materials. Using MoS_2 as an example, we report ultrafast and efficient charge transfer between $MoTe_2$ and MoS_2 monolayers. In the transient absorption measurements, an ultrashort pump pulse is used to selectively excite electrons in $MoTe_2$. The appearance of the excited electrons in the conduction band of MoS_2 is monitored by using a probe pulse that is tuned to the resonance of MoS_2. We found that electrons transfer to MoS_2 on a time scale of at most 0.3 ps. The transferred electrons give rise to a large transient absorption signal at both A-exciton and B-exciton resonances due to the screening effect. We also observed ultrafast transfer of holes from MoS_2 to $MoTe_2$. Our results suggest the feasibility of using $MoTe_2$ as a bridge material to connect MoS_2 and other transition metal dichalcogenides, and demonstrate a new transition metal dichalcogenide heterostructure involving $MoTe_2$, which extends the spectral range of such structures to infrared.

1. Introduction

The newly developed two-dimensional (2D) materials, such as transition metal dichalcogenides (TMDs), have shown great potential in electronic and optoelectronic applications [1–4]. However, one key challenge is the large contact resistance between 2D materials and metal electrodes due to the Schottky nature of the contacts [5]. In Si-based technology, the ohmic contact can be readily achieved via doping; however, this approach is less effective in 2D materials, and there appears to be a fundamental difficulty in achieving low contact resistance between the 2D material and metal. A less explored member of TMD family, $MoTe_2$, can potentially offer a solution to this critical issue.

Recent photoluminescence (PL) and absorption experiments have shown that monolayer (ML) $MoTe_2$ is a direct semiconductor with an optical band gap of about 1.1 eV [6–8]. Since the most studied TMDs, such as MoS_2, $MoSe_2$, WS_2 and WSe_2, have optical band gaps in the visible range [1], $MoTe_2$ offer to extend optoelectronic applications of TMDs to the infrared range. Unlike most TMDs that become indirect in multilayer forms, $MoTe_2$ retains its direct nature in bilayers, and perhaps even in trilayers [7]. Optical measurements, such as Raman spectroscopy [9–12] and temperature-dependent PL spectroscopy [13], have revealed lattice vibration and exciton dephasing properties of ML and multilayer $MoTe_2$. On electronic applications, multilayer $MoTe_2$ field-effect transistors have been fabricated with relatively high on/off ratios [14–18]. Un-gated $MoTe_2$ shows p-type conductivity [14]; however, ambipolar transport has also been demonstrated [16, 19, 20]. Other potential applications of $MoTe_2$ as environmental sensors [21] and photodetectors [22, 23] were also explored. Furthermore, $MoTe_2$ was found to possess other elusive properties such as giant and tunable valley degeneracy splitting [24], strong spin-polarization effects [25], and superconductivity phase [26]. Related to the

application prospects, significant progress has been made on fabricating large area and high quality $MoTe_2$ by chemical vapor deposition [27, 28] and molecular beam epitaxy [29, 30].

In addition to being an infrared responsive TMD, an even more promising aspect of $MoTe_2$ is its potential to serve as a contacting material for other 2D materials. First-principle calculations have indicated that $MoTe_2$ is a phase transition material that can transform from monoclinic (1*T*) metallic to hexagonal (2*H*) semiconducting phases by deformation [31] or gating [32]. A recent experiment demonstrated, through laser-induced phase transition, that an ohmic heterophase homojunction between semiconducting and metallic $MoTe_2$ MLs can be formed [33]. The processed materials were found to be stable up to room temperature, with a carrier mobility improved by a factor of about 50, while retaining a high current on/off ratio of 10^6 [33, 34].

We propose to use $MoTe_2$ as an intermediate material to make contacts with other 2D materials, especially other TMDs. In such structures, a phase-patterned $MoTe_2$ ML is used between a metal and another TMD ML. The metal electrode is connected to the metallic region of $MoTe_2$, while the semiconducting phase makes contact with the other 2D semiconductor. To successfully employ $MoTe_2$ as a connecting material, charge should efficiently be transferred between semiconducting $MoTe_2$ and other semiconducting 2D materials. Here we demonstrate ultrafast charge transfer between a semiconducting $MoTe_2$ ML and a MoS_2 ML. A van der Waals bilayer of $MoTe_2$–MoS_2 was fabricated by mechanical exfoliation followed by a dry transfer process. Charge carrier dynamics in such a structure was studied by ultrafast transient absorption measurements. We found that electrons excited in $MoTe_2$ transfer to MoS_2 on a sub-picosecond time scale. The transfer of holes from MoS_2 to $MoTe_2$ was also found to be ultrafast. These results suggest the feasibility of using $MoTe_2$ as a channel material for electric contacting TMD MLs.

We choose MoS_2 as the material to interface with $MoTe_2$ for two reasons. First, MoS_2 is the most extensively studied TMD to date, especially on its transport properties. Second, MoS_2 itself have also shown phase engineering potentials that achieve low resistance between its metallic and semiconducting phases [35]. Based on first-principle calculations, $MoTe_2$ and MoS_2 form a type-II band alignment, with the conduction band minimum (CBM) and valance band maximum located in MoS_2 and $MoTe_2$ layers, respectively [36]. The predicted energy levels with respect to the vacuum level are schematically shown in figure 1(a). This type-II band alignment facilitates the transfer of electrons from $MoTe_2$ to MoS_2 and holes along the opposite direction.

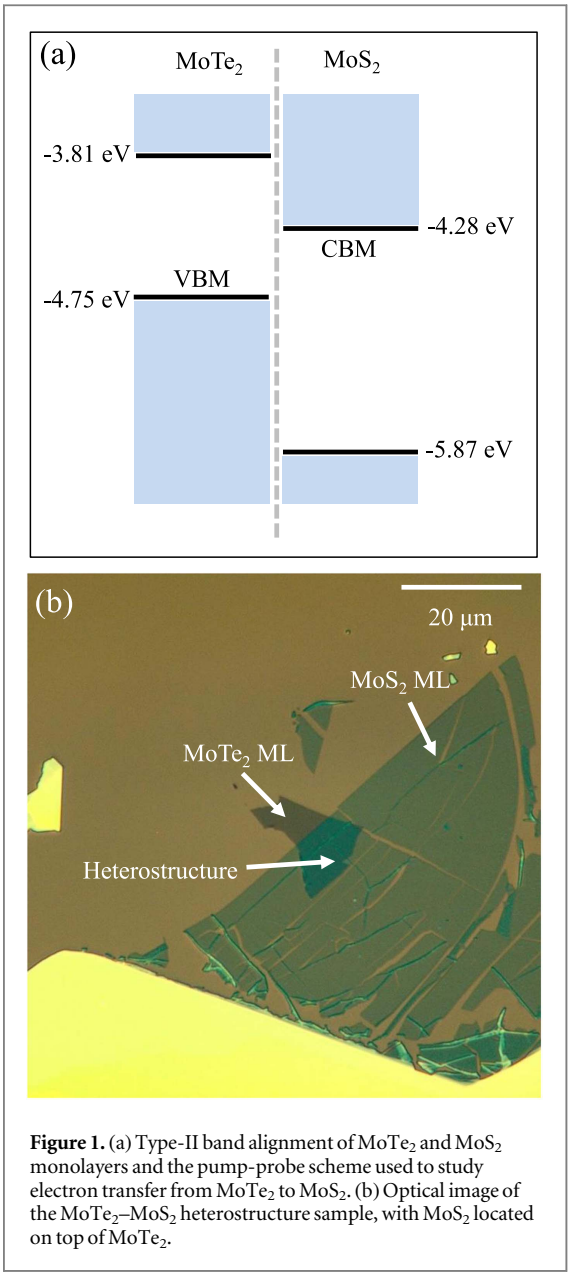

Figure 1. (a) Type-II band alignment of $MoTe_2$ and MoS_2 monolayers and the pump-probe scheme used to study electron transfer from $MoTe_2$ to MoS_2. (b) Optical image of the $MoTe_2$–MoS_2 heterostructure sample, with MoS_2 located on top of $MoTe_2$.

2. Experimental procedures

The $MoTe_2$–MoS_2 heterostructures were fabricated as follows: both MoS_2 and $MoTe_2$ ML flakes were fabricated onto PDMS substrates by a standard mechanical exfoliation procedure using adhesive tapes. Then, the MLs were transferred sequentially to a Si/SiO_2 substrate where part of the $MoTe_2$ ML was covered by the MoS_2 ML. For the purpose of studying interlayer charge transfer, we do not expect the sequence of the two layers to play a significant role. Since MoS_2 is expected to be more stable in ambient conditions, to protect the $MoTe_2$ layer from degradation, the MoS_2 layer is place on top. In order to clean the interface between the two MLs, which is important for efficient charge transfer, the samples were thermally annealed at 200 °C for 2 h under a H_2–Ar (20–100 sccm) environment at a base pressure of about 3 Torr. Two samples with the same structure

were investigated and similar results were obtained. Here we present results from the relatively large sample shown in figure 1(b). This sample also contains large areas of $MoTe_2$ and MoS_2 MLs, which facilitate the direct comparison between the heterostructure and the constituent MLs.

The transient absorption setup employs a Ti:sapphire laser system with an 80 MHz repetition rate and a 100 fs pulse duration. The output of the Ti:sapphire laser with a central wavelength of 800 nm is split into two parts. One part is directly used in the measurement. The other part is coupled to a photonic crystal fiber, from which a broadband supercontinuum from 500 to 1200 nm is obtained. A dielectric bandpass filter with a bandwidth of 10 nm is utilized to select a specific wavelength component used in the measurement. In a certain measurement, one of these pulses is used as the pump, while the other as the probe. The pulse serving as the pump is modulated by a mechanical chopper at about 2.4 KHz. The pump and the probe beams, after independent adjustment of their power, polarization and travel length, are combined by a beamsplitter and focused on the sample by a microscope objective with a numerical aperture of 0.4. The reflected probe beam was measured by a photodiode and a lock-in amplifier. All the measurements were performed under ambient condition. By using this setup, we can measure the differential reflection as a function of the probe delay, that is, the time lag of the probe pulse with respect to the pump pulse.

3. Results and discussion

In the transient absorption measurements, carriers are injected by a pump pulse, and detected by measuring a differential reflection, which is defined as the normalized difference between the reflection of the probe pulse by the sample with (R) and without (R_0) the presence of the pump pulse, $\Delta R/R_0 = [R - R_0]/R_0$. This quantity measures the relative change of the complex index of refraction of the sample at the probe wavelength induced by the carriers injected by the pump pulse. The precise relations between the differential reflection and the changes in the absorption coefficient and index of refraction can be rather complex if multiple reflections from the sample and the substrate are involved [37]. However, for small changes ($\Delta R/R_0 \ll 1$), a linear relation can be assumed [37]. Furthermore, for relatively low carrier densities, the changes in the absorption coefficient and the index of refraction can be treated as being proportional to the carrier density [38].

As the starting point, we first investigated the $MoTe_2$ ML region. A pump pulse of 1.88 eV was used to excite the sample, as schematically illustrated by the blue vertical arrow in the inset of figure 2(d). The black squares in figures 2(a) and (b) show the differential reflection signal of a 1.55 eV probe, measured with a pump fluence of 3.5 μJ cm^{-2}. By using an absorption coefficient of 3×10^6 cm^{-1} (at 1.88 eV) [6], the injected carrier density is estimated to be about 2×10^{12} cm^{-2}. Since the optical bandgap of $MoTe_2$ ML is about 1.1eV, the pump injects hot carriers with excess energies of a few hundred millielectrovolts, while the probe senses states near the bandedges. As shown in figure 2(a), the signal reaches a peak rapidly and is followed by a fast decay process. We attribute this feature to the energy relaxation of hot carriers and exciton formation: the initial nonthermal carrier distribution injected by the pump pulse quickly evolves to a hot Fermi–Dirac distribution. The relaxation of the hot carriers into the states near the bandedges give rise to the increase of the signal. The further energy relaxation of carriers to lower energy states and the exciton formation processes rapidly decrease the population of states being probed and hence the initial fast decay of the signal. After this transient process, the carriers reached thermal equilibrium and are predominately in the form of excitons.

The rest of the decay is a simple single exponential process, as shown by the solid curves in figure 2(b), due to exciton recombination. We obtained a decay time constant of about 60 ps. Such a short lifetime indicates that the exciton lifetime is limited by the nonradiative recombination induced by defects. When the pump fluence is changed, we observed similar dynamics, as indicated by the red and blue symbols in figures 2(a) and (b). The signal at 1 ps, that is, after the short transient, is proportional to the pump fluence, as shown by the red circles in figure 2(c). This confirms that the measurement is performed in the regime where the differential reflection is proportional to the carrier density, as we discussed in the previous paragraph. We note that the slope indicates that an exciton density of 1×10^{12} cm^{-2} gives rise to a differential reflection signal of about 0.9×10^{-3}. The peak signal appears to be sub-linear with the pump fluence (black squares), and can be attributed to the fact that this quantity is influenced by the thermalization and relaxation processes; therefore, it does not truly reflect the injected density. Finally, the decay time constant is independent of the pump fluence, as shown in figure 2(d). Such a density-independent decay process suggests that the exciton–exciton annihilation is absent in this material. It is interesting to note that such a process have been observed in other TMD MLs with the same levels of injection densities [39–43].

We next study the electron transfer from $MoTe_2$ to MoS_2 in the heterostructure. We selectively excite electrons to the conduction band of $MoTe_2$ with a 1.55 eV pump pulse, as shown by the blue vertical arrow in the inset of figure 3(b). The pump photon energy is not enough to excite the MoS_2 layer, which has the lowest exciton energy larger than 1.80 eV. Hence, only the $MoTe_2$ is excited. From the pump fluence of 2.4 μJ cm^{-2} and an absorption coefficient of 2×10^6 cm^{-1} (at 1.55 eV), [6] we estimate that the

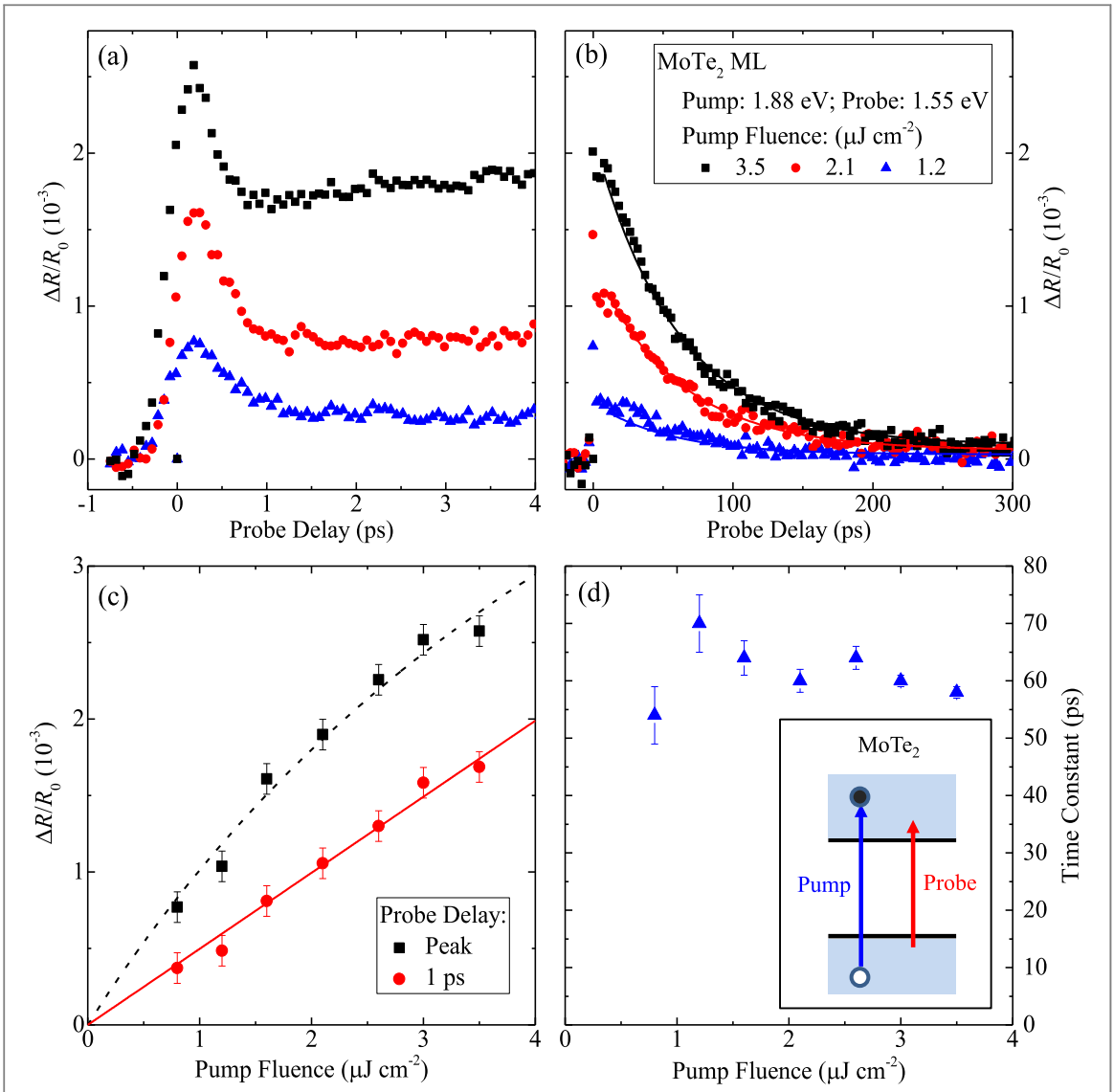

Figure 2. Differential reflection signal measured with a $MoTe_2$ monolayer (ML) sample with a pump of 1.88 eV and a probe of 1.55 eV. (a) and (b) Show the short and long time ranges of the signal, respectively. The black, red, and blue symbols correspond to pump fluence values of 3.5, 2.1 and 1.2 μJ cm^{-2}, respectively. The solid lines are exponential fits. (c) The peak differential reflection signal (black squares) and that at a probe delay of 1 ps (red circles) as a function of the pump fluence. The red line is a linear fit. (d) The decay time constant of the differential reflection signal as a function of the pump fluence.

pump pulse injects electron–hole pairs in $MoTe_2$ with a peak density of 1.2×10^{12} cm^{-2}. Once injected, electrons are expected to move to the MoS_2 layer, where the CBM resides, as indicated by the dashed arrow in the inset of figure 3(b). This electron transfer process was monitored by a probe pulse tuned to the A-exciton resonance, 1.88 eV, as shown by the red vertical arrow in the inset of figure 3(b). The black symbols in figure 3 show the measured differential reflection signal over short (a) and long (b) time scales, respectively. The signal reaches a peak in about 0.3 ps and then decays single exponentially with a time constant of 6 ± 1 ps, which was deduced from an exponential fit (solid curve). When the probe photon energy was changed, the same dynamics were observed; however, both the magnitude and the sign of the signal change dramatically. The peak values of the signal with various probe photon energies are summarized by the symbols in figure 3(c), along with a PL spectrum obtained from a MoS_2 ML sample (the curve).

The results summarized in figure 3 show unambiguously the ultrafast and efficient electron transfer process from $MoTe_2$ to MoS_2. First, the strong dependence of the signal on the probe photon energy around the exciton resonance of MoS_2 confirms that the probe detects carriers in MoS_2. Although the probe photon energy is higher than the bandgap of $MoTe_2$, the additional signal provided by the carriers in $MoTe_2$ plays a negligible role; otherwise, the signal would have been independent of the probe photon energy in this spectrum range. Since the MoS_2 layer is not excited, the electrons detected in the conduction band of MoS_2 can only be those excited in $MoTe_2$ and sequentially transferred to MoS_2 across the van der Waals interface. Control experiments performed on the $MoTe_2$ and

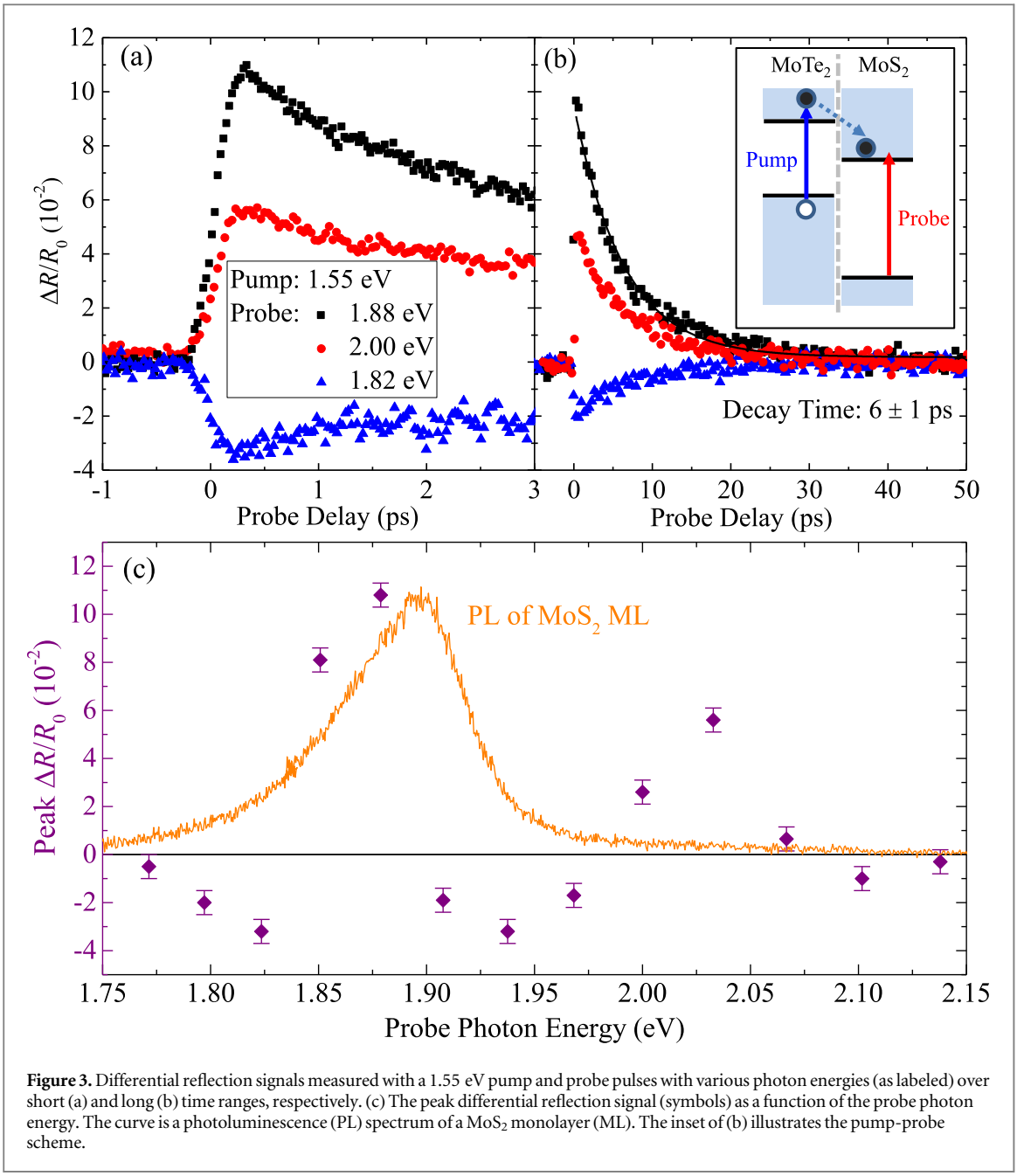

Figure 3. Differential reflection signals measured with a 1.55 eV pump and probe pulses with various photon energies (as labeled) over short (a) and long (b) time ranges, respectively. (c) The peak differential reflection signal (symbols) as a function of the probe photon energy. The curve is a photoluminescence (PL) spectrum of a MoS_2 monolayer (ML). The inset of (b) illustrates the pump-probe scheme.

MoS_2 ML regions of the sample produced no detectable signal. The observed rising time of the signal of 0.3 ps is close to the time resolution of the instrument. This indicates that the upper limit of the electron transfer time is 0.3 ps.

The decay of the signal reflects the lifetime of the transferred electrons in MoS_2. Interestingly, the time constant of 6 ps is about 10 times shorter than the lifetimes of excitons in $MoTe_2$ MLs of about 60 ps (figure 2). We attribute this short lifetime to recombination of electrons with background holes in MoS_2. It was known that $MoTe_2$ is naturally p-doped. Once the heterostructure is formed, the holes in $MoTe_2$ can move to MoS_2, resulting in background holes in MoS_2. The transferred electrons then can recombine with these holes. The short lifetime observed here is also strikingly different from previous studied TMD heterostructures, where extremely long lifetimes were observed due to the lack of recombination partners as the electrons and hole populate different layers [44, 45].

We found that the induced differential reflection signal is surprisingly large and show rich spectral features. As the probe photon energy is changed, both photoinduced bleaching (positive signal) and photoinduced absorption (negative signal) were observed. The two peaks at about 1.88 and 2.03 eV are well aligned with the A and B exciton transitions of MoS_2 MLs [46], showing that the electrons transferred to MoS_2 alter the two excitonic transitions with similar magnitudes. Assuming all the excited electrons transfer to MoS_2, the electron density of 1.2×10^{12} cm^{-2} induces a differential reflection signal as large as 10^{-1}. In comparison, electron–hole pairs or excitons

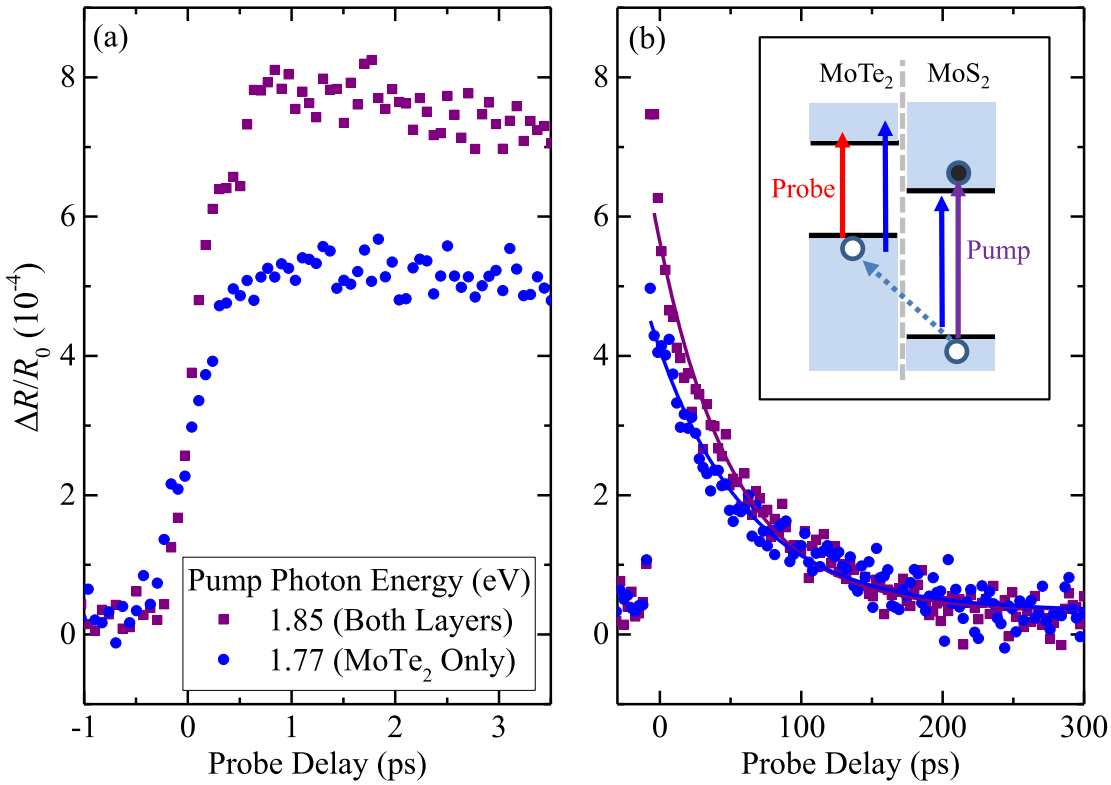

Figure 4. Differential reflection signals measured with a 1.55 eV probe over short (a) and long (b) time scales. The pump photon energies are 1.85 (purple squares) and 1.77 eV (blue circles), respectively. The solid lines are exponential fits. The inset of (b) illustrates the pump-probe scheme.

injected in MoS_2 MLs with such a density only give rise to a signal on the order of 10^{-3} [39, 47, 48]. These features suggest that the transferred electrons induce the differential reflection signal mainly through screening instead of phase state filling effects: to screen the Coulomb interaction in excitons, charged carriers of one type are expected to be more efficient than the neutral electron-hole pairs with the same density.

Due to the type-II band alignment shown in figure 1(a), holes in MoS_2 are expected to move to $MoTe_2$, opposite to the electron motion. To study the transfer of holes from MoS_2 to $MoTe_2$, we excite the MoS_2 layer and probe $MoTe_2$. This configuration is schematically shown in the inset of figure 4(b). However, since the bandgap of MoS_2 is larger than that of $MoTe_2$, any pump that is energetic enough to excite MoS_2 will inevitably excited $MoTe_2$ layer, making the analysis of the result more complicated. To separate the effects of photocarriers directly injected in the $MoTe_2$ layer of the heterostructure and those transferred from MoS_2, we first used a pump pulse of 1.77 eV (blue vertical arrow), which is lower than the optical bandgap of MoS_2 and hence can only excite $MoTe_2$. From its fluence of 1.6 μJ cm^{-2}, the estimated injected density is about 1×10^{12} cm^{-2}. The blue circles in figure 4 show the differential reflection signal measured with a probe of 1.55 eV. As the probe photon energy is much lower than optical bandgap of MoS_2, it can only probe the $MoTe_2$ layer (red vertical arrow). Since the electrons excited in $MoTe_2$ transfer to MoS_2, and hence become invisible to the 1.55 eV probe, the signal is induced by the holes excited in $MoTe_2$. According to figure 2, an exciton density of 1×10^{12} cm^{-2} induces a differential reflection of the 1.55 eV probe of 0.9×10^{-3} in $MoTe_2$ ML. The observed signal of about 0.5×10^{-3} is reasonably consistent with that value, considering half of the carriers (electrons) have left $MoTe_2$. As shown the figure 4(b), the signal decays exponentially, with a time constant of about 62 ps (the blue curve). This decay time is also consistent with the exciton lifetime in $MoTe_2$.

Finally, we change the pump photon energy to 1.85 eV, so that it can excite both layers (purple vertical arrow in the inset of figure 4(b)). The results are shown as the purple squares. From 1.77 to 1.85 eV, the change of the absorption coefficient of $MoTe_2$ is at most a few per cent [6]. The increase of the signal can only be attributed to the excitation of MoS_2. The absorption coefficients of MoS_2 and $MoTe_2$ at 1.85eV are 0.4×10^6 and 3×10^6 cm^{-1}, respectively. From these values, one would expect that the holes excited in MoS_2 that transferred to $MoTe_2$ to increase the signal by about 13%, smaller than what was shown in figure 4. We attribute the discrepancy to the uncertainties about the relative values of the absorption coefficients, the interference effect of the substrate that changes the reflectivity, and the fact that MoS_2 layer is

on top of $MoTe_2$, and therefore attenuate the pump reaching $MoTe_2$. Nevertheless, the increased signal indicates the existence of the hole transfer process. The ultrafast rising time observed with the 1.85 eV pump indicates that the hole transfer time is shorter than 0.5 ps. The decay of the signal is about 55 ps, as indicated by the purple curves in figure 4(b), which is reasonably consistent with the result of 1.77 eV pump.

4. Conclusion

We observed subpicosecond transfer of electrons and holes between MoS_2 and $MoTe_2$. A van der Waals heterostructure composed of MoS_2 and $MoTe_2$ MLs was fabricated by mechanical exfoliation of bulk crystals followed by a dry transfer process. By selectively exciting electrons in the $MoTe_2$ layer with an ultrashort laser pulse and monitoring the appearance of these electrons in MoS_2 with a probe pulse, we obtained evidence of an ultrafast electron transfer processes. Ultrafast hole transfer from MoS_2 to $MoTe_2$ was also observed in a similar way. Since phase engineering has been demonstrated to be effective in achieving ohmic contact between metallic and semiconducting $MoTe_2$, our observation of the efficient and ultrafast charge transfer between $MoTe_2$ and MoS_2 indicates the feasibility of using $MoTe_2$ as a bridge material to connect MoS_2 as well as other TMDs. Our result also demonstrated a new TMD heterostructure involving $MoTe_2$, which extends the spectral range of such structures to infrared.

Acknowledgments

SP acknowledges Shandong Province Natural Science Foundation (Project ZR2014FM037) and National Nature Science Foundation of China (Project 11274188). HZ is supported by the National Science Foundation of USA under Award Nos. DMR-1505852 and IIA-1430493.

References

[1] Wang Q H, Kalantar-Zadeh K, Kis A, Coleman J N and Strano M S 2012 *Nat. Nanotechnol.* **7** 699–712
[2] Bhimanapati G R *et al* 2015 *ACS Nano* **9** 11509–39
[3] Mak K F and Shan J 2016 *Nat. Photon.* **10** 216–26
[4] Zhang W, Wang Q, Chen Y, Wang Z and Wee A T S 2016 *2D Mater.* **3** 022001
[5] Allain A, Kang J H, Banerjee K and Kis A 2015 *Nat. Mater.* **14** 1195–205
[6] Ruppert C, Aslan O B and Heinz T F 2014 *Nano Lett.* **14** 6231–6
[7] Lezama I G, Arora A, Ubaldini A, Barreteau C, Giannini E, Potemski M and Morpurgo A F 2015 *Nano Lett.* **15** 2336–42
[8] Yang J, Lu T, Myint Y W, Pei J, Macdonald D, Zheng J C and Lu Y 2015 *ACS Nano* **9** 6603–9
[9] Yamamoto M, Wang S T, Ni M, Lin Y F, Li S L, Aikawa S, Jian W B, Ueno K, Wakabayashi K and Tsukagoshi K 2014 *ACS Nano* **8** 3895–903
[10] Froehlicher G, Lorchat E, Fernique F, Joshi C, Molina-Sanchez A, Wirtz L and Berciaud S 2015 *Nano Lett.* **15** 6481–9
[11] Park J, Kim Y, Jhon Y I and Jhon Y M 2015 *Appl. Phys. Lett.* **107** 153106
[12] Song Q J, Tan Q H, Zhang X, Wu J B, Sheng B W, Wan Y, Wang X Q, Dai L and Tan P H 2016 *Phys. Rev.* B **93** 115409
[13] Koirala S, Mouri S, Miyauchi Y and Matsuda K 2016 *Phys. Rev.* B **93** 075411
[14] Fathipour S, Ma N, Hwang W S, Protasenko V, Vishwanath S, Xing H G, Xu H, Jena D, Appenzeller J and Seabaugh A 2014 *Appl. Phys. Lett.* **105** 192101
[15] Pradhan N R, Rhodes D, Feng S, Xin Y, Memaran S, Moon B H, Terrones H, Terrones M and Balicas L 2014 *ACS nano* **8** 5911
[16] Xu H, Fathipour S, Kinder E W, Seabaugh A C and Fullerton-Shirey S K 2015 *ACS Nano* **9** 4900–10
[17] Pezeshki A, Shokouh S H H, Jeon P J, Shackery I, Kim J S, Oh I K, Jun S C, Kim H and Im S 2016 *ACS Nano* **10** 1118–25
[18] Lezama I G, Ubaldini A, Longobardi M, Giannini E, Renner C, Kuzmenko A B and Morpurgo A F 2014 *2D Mater.* **1** 021002
[19] Lin Y F *et al* 2014 *Adv. Mater.* **26** 3263–9
[20] Nakaharai S, Yamamoto M, Ueno K, Lin Y F, Li S L and Tsukagoshi K 2015 *ACS Nano* **9** 5976–83
[21] Lin Y F, Xu Y, Lin C Y, Suen Y W, Yamamoto M, Nakaharai S, Ueno K and Tsukagoshi K 2015 *Adv. Mater.* **27** 6612–9
[22] Kuiri M, Chakraborty B, Paul A, Das S, Sood A K and Das A 2016 *Appl. Phys. Lett.* **108** 063506
[23] Zhang K A *et al* 2016 *ACS Nano* **10** 3852–8
[24] Qi J S, Li X, Niu Q and Feng J 2015 *Phys. Rev.* B **92** 121403
[25] Zhang Q Y, Yang S Y A, Mi W B, Cheng Y C and Schwingenschlogl U 2016 *Adv. Mater.* **28** 959–66
[26] Qi Y P *et al* 2016 *Nat. Commun.* **7** 11038
[27] Park J C, Yun S J, Kim H, Park J H, Chae S H, An S J, Kim J G, Kim S M, Kim K K and Lee Y H 2015 *ACS Nano* **9** 6548–54
[28] Zhou L *et al* 2015 *J. Am. Chem. Soc.* **137** 11892–5
[29] Diaz H C, Chaghi R, Ma Y J and Batzill M 2015 *2D Mater.* **2** 044010
[30] Roy A, Movva H C P, Satpati B, Kim K, Dey R, Rai A, Pramanik T, Guchhait S, Tutuc E and Banerjee S K 2016 *ACS Appl. Mater. Interfaces* **8** 7396–402
[31] Duerloo K A, Li Y and Reed E J 2014 *Nat. Commun.* **5** 4214
[32] Li Y, Duerloo K A N, Wauson K and Reed E J 2016 *Nat. Commun.* **7** 10671
[33] Cho S *et al* 2015 *Science* **349** 625–8
[34] Keum D H *et al* 2015 *Nat. Phys.* **11** 482–7
[35] Kappera R, Voiry D, Yalcin S E, Branch B, Gupta G, Mohite A D and Chhowalla M 2014 *Nat. Mater.* **13** 1128–34
[36] Kang J, Tongay S, Zhou J, Li J B and Wu J Q 2013 *Appl. Phys. Lett.* **102** 012111
[37] Wang R, Ruzicka B A, Kumar N, Bellus M Z, Chiu H Y and Zhao H 2012 *Phys. Rev.* B **86** 045406
[38] Schmitt-Rink S, Chemla D S and Miller D A B 1985 *Phys. Rev.* B **32** 6601–9
[39] Sun D, Rao Y, Reider G A, Chen G, You Y, Brezin L, Harutyunyan A R and Heinz T F 2014 *Nano Lett.* **14** 5625–9
[40] Kar S, Su Y, Nair R R and Sood A K 2015 *ACS Nano* **9** 12004–10
[41] Kumar N, Cui Q, Ceballos F, He D, Wang Y and Zhao H 2014 *Phys. Rev.* B **89** 125427
[42] Yuan L and Huang L B 2015 *Nanoscale* **7** 7402–8
[43] Mouri S, Miyauchi Y, Toh M, Zhao W, Eda G and Matsuda K 2014 *Phys. Rev.* B **90** 155449
[44] Hong X, Kim J, Shi S F, Zhang Y, Jin C, Sun Y, Tongay S, Wu J, Zhang Y and Wang F 2014 *Nat. Nanotechnol.* **9** 682–6
[45] Ceballos F, Bellus M Z, Chiu H Y and Zhao H 2014 *ACS Nano* **8** 12717–24
[46] Mak K F, Lee C, Hone J, Shan J and Heinz T F 2010 *Phys. Rev. Lett.* **105** 136805
[47] Shi H, Yan R, Bertolazzi S, Brivio J, Gao B, Kis A, Jena D, Xing H G and Huang L 2012 *ACS Nano* **7** 1072–80
[48] Pogna E A A *et al* 2016 *ACS Nano* **10** 1182–8